A NON-FRACTAL CHAOTIC ATTRACTOR ON A TWO-DIMENSIONAL SURFACE

by

Gui-nian Lin and Leon O. Chua

A NON-FRACTAL CHAOTIC ATTRACTOR
ON A TWO-DIMENSIONAL SURFACE

by

Gui-nian Lin and Leon O. Chua

Memorandum No. UCB/ERL M91/32

1 March 1991

ELECTRONICS RESEARCH LABORATORY

A NON-FRACTAL CHAOTIC ATTRACTOR
ON A TWO-DIMENSIONAL SURFACE †

Gui-nian Lin †† and Leon O. Chua †††

ABSTRACT

In this paper we report a non-fractal chaotic attractor observed in a third-order piecewise-linear circuit. The attractor's Lyapunov exponents and spectrum show that it is chaotic, while its trajectory is ergodic on a 2-dimensional surface and therefore this attractor does not possess a fractal structure.

A special 2-dimensional surface called a *folded strip* is introduced to explain the geometrical structure of the attractor. Using a 1-dimensional map, it is proved that trajectories on a folded strip can be chaotic. This explains the chaotic mechanism of the attractor.

The attractor's Lyapunov dimension, capacity dimension and correlation dimension have been calculated and compared. It is shown that the Kaplan-Yorke conjecture does not hold for this attractor.

1. Introduction

Chaos and Strange attractors have been hot research topics for years. Most chaotic attractors observed so far, either from discrete maps or from continuous flows, are strange attractors. Consequently, the terms *chaotic attractor* and *strange attractor* are often abused and used as synonyms. However, in a strict sense, chaotic attractors need not be strange and strange attractors need not be chaotic([1][2]). We adopt the definition for chaotic attractors and strange attractors, from [1]. Roughly speaking, the term "chaotic" is more *dynamics* oriented. It implies sensitive dependence on initial conditions. A mathematical criterion is that at least one Lyapunov exponent of the attractor is positive. The term "strange" is more *geometry* oriented. It means the attractor has a rather exotic geometrical structure, such as a noninteger fractal dimension, a self-similar Cantor set anatomy, etc. In this paper we report an example of a non-strange chaotic attractor observed from a third-order piecewise-linear circuit, i.e. the canonical realization of the Chua's circuit family([3]). Non-strange attractors have been reported for discrete maps([1][2]). Ours is probably the first example of a non-strange attractor observed in vector fields of continuous flow.

In *Section* 2 we present the trajectory of the attractor and its Poincare cross-sections derived from computer simulations. From these numerically derived Poincare cross-sections it appears that the trajectory is located on a 2-dimensional surface and that it is ergodic on this surface. In *Section* 3 we calculate the Lyapunov exponents and the spectrum of the attractor to show that it is chaotic. In *Section* 4 we present a special geometrical structure of a 2-dimensional surface called a *folded strip,* and explain why a trajectory traveling on it can be chaotic. In *Section* 5 we present experimental observations on the same attractor and therefore show that this attractor is really observable in *physical* systems. Finally in *Section* 6 we discuss the problem of dimension. By calculating and comparing the attractor's Lyapunov dimension, capacity dimension and correlation dimension, it appears that this attractor provides a counter-example to the Kaplan-Yorke conjecture([4]).

2. Trajectory and Poincare Cross-sections

The six-element circuit shown in Fig.1(a) is a canonical realization of the Chua's circuit family. Fig.1(b) shows the v-i characteristic of the piecewise-linear resistor R_N in Fig.1(a). The state equations of the circuit in Fig.1(a) are

$$\frac{dv_1}{dt} = \frac{1}{C_1}[-f(v_1) + i_3]$$

$$\frac{dv_2}{dt} = \frac{1}{C_2}(-Gv_2 + i_3)$$ (1)

$$\frac{di_3}{dt} = \frac{-1}{L}(v_1 + v_2 + Ri_3)$$

where

$$f(v) = G_b v + \frac{1}{2}(G_a - G_b)[|v + 1| - |v - 1|]$$ (2)

is the v-i characteristic of the nonlinear resistor shown in Fig.1(b).

[Figure 1]

For the particular attractor discussed in this paper, the parameter values are:

$$C_1 = 1.0, \quad C_2 = -15.6, \quad G = -6.42,$$

$$G_a = 4.13, \quad G_b = 0.906, \quad L = 0.42, \quad R = -0.555$$ (3)

By plotting the trajectory of Eq.(1) with the parameter values given in (3), we obtain the attractor shown in Fig.2 in three different projections, where

$$x[1] = v_1, \quad x[2] = v_2, \quad x[3] = i_3.$$

The software we use is INSITE([5][6]).

[Figure 2]

As seen from the figure, the attractor looks like a strip. To explore its geometrical structure further, we plotted its Poincare cross-sections at several different positions. Fig.3 shows a cross-section at $v_2 = 0$ plane. Observe that this cross-section consists of two continuous curves. In fact, we have found, not only this one, but all Poincare cross-sections from any directions consist of one or more continuous curves. Therefore, within the numerical accuracy of our computer (DECstation3100), it appears that this attractor is located on a 2-dimensional surface and does not have a fractal structure.

[Figure 3]

3. Lyapunov Exponents and Spectrum

Our numerical results on the trajectory and the Poincare cross-sections have revealed a 2-dimensional geometrical structure for this attractor. In order to learn more about its dynamical behavior, let us investigate its Lyapunov exponents and spectrum in this Section.

Our algorithm for calculating the Lyapunov exponents is based on the Gram-Schmidt orthonormalization technique[6]. Starting from an initial condition close to the attractor, using more than 50000 data points obtained from the Runge-Kutta integration routine, this algorithm for calculating Lyapunov exponents converges very well. The results listed below are virtually independent from the initial conditions used for the algorithm.

$$l_1 = 0.0345 \, , \quad l_2 = -0.0000751 \, , \quad l_3 = -0.755 \qquad (4)$$

From a practical point of view, we can classify them as follow:

$$l_1 > 0 \, , \quad l_2 = 0 \, , \quad l_3 < 0 \qquad (5)$$

It is quite reasonable that the attractor has one Lyapunov exponent equal to zero([7]). The negative Lyapunov exponent l_3 has the largest absolute value, thereby implying that the trajectory converges to an attractor. The most important point is that this attractor has a positive Lyapunov exponent, thereby suggesting that it is chaotic.

Another numerical criterion for asserting that the attractor is chaotic, and not quasi-periodic, or periodic with a long period, is its spectrum. Figure 4 shows the spectrum obtained by using FFT analysis with 2^{16} data points from the time waveform of v_1 associated with the attractor. The spectrum has components over a broad band of frequencies, and hence meeting our second empirical characterization for chaotic attractors. The highest peak 5.2dB appears at $f \approx 0.08Hz$. This corresponds to the time needed for a point traveling one cycle along the trajectory (see Fig.2), which is averagely $T \approx 12sec$. Since the attractor is asymmetric with respect to the origin, the spectrum has a nonzero component, -3.2dB, at $f = 0$. In Fig.4, this component coincides with the vertical axes, and hence cannot be distinguished clearly. The spectra for v_2 and i_3 are qualitatively similar to that of v_1 and we therefore omitted them.

Therefore, both the Lyapunov exponents and the spectrum indicate that this attractor is chaotic.

Figure 4

4. Geometrical Explanation

It is well known that the most complicated attractors existing in any 2-dimensional autonomous dynamical systems can only be limit cycles. In other words, any attractors on a 2-dimensional plane can only be either equilibrium points or limit cycles, because the trajectory can never intersect itself on a plane, except at equilibrium points. Consequently, in order for our chaotic attractor to be 2-dimensional, it must sit on some *non-planar* 2-dimensional surface.

In this Section we will describe a 2-dimensional surface with a special geometrical structure and prove that a trajectory on it can be chaotic.

Let us start with a long strip of paper(with no thickness), as shown in Fig.5(a). Imagine first that we band it around into a cylinder by pasting the line AC to the line GH. The result is an orientable cylindrical *closed-strip*. Let us define a continuous vector field (with no equilibrium points) on this cylindrical closed-strip. Without loss of generality, we can assume the lines AG and CH are in parallel with the vector field. If they are not, we can tailor the closed-strip to make so. When a trajectory evolves along this closed-strip, we claim that the only possible attractors are limit cycles. We can prove this assertion by introducing a 1-dimensional map as follow: first, label the line GH as the x axis, with $x_G = 0$ and $x_H = 1$, as shown in Fig.5(a). Suppose next that a trajectory starting from an arbitrary point x_0 on GH arrives at some point x_1 on AC. Since the line AC is identified with the line GH, the point x_1 is also a point on GH. Therefore we get a 1-dimensional map $f_0: x_0 \rightarrow x_1$. The map f_0 is continuous and monotone-increasing because the vector field on a plane can never intersect itself. Figure 6(a) shows a typical continuous monotone-increasing map. Clearly, it can have one or more stable and/or unstable fixed points. Each of the stable fixed points (with $|df/dx| \leq 1$) corresponds to a periodic motion of the trajectory on the closed-strip.

Next imagine that we twist the plain strip in Fig.5(a) by 180 degrees and paste the line AC upside down to the line HG (i.e. paste point A to point H and paste point C to point G). We then get a *Möbius strip*. Again, let us analyze the trajectories on it by using a 1-dimensional map f_1. Suppose a trajectory starting from the point x_0 arrives at some point x_1 on AC in Fig.5(a). Due to the fact that the line AC is pasted upside down to the line HG, the point x_1 is now identified with the point x_1' on GH so that

$$|1-x_1| = |x_1'|$$

in Fig.5(a). Therefore the map $f_1: x_0 \rightarrow x_1'$ is continuous and monotone-decreasing. Figure 6(b) shows a typical continuous monotone-decreasing map. Obviously, a

monotone-decreasing map has only one intersecting point with the diagonal line. If we have $|df_1/dx| \leq 1$ at this intersecting point, then there is a stable periodic trajectory on the strip. Therefore, although the Möbius strip seems to be more complicated then the flat closed-strip, still, the only possible attractors on it is a limit cycle.

Now suppose we fold the long strip in Fig.5(a) along the line BE and paste the rectangle ADEB to the rectangle CFEB. The result is a spoon-like shape structure henceforth referred to as a *folded junction*, as shown in Fig.5(b). Imagine next that we stretch the whole strip continuously (as if it were a rubber band) and band it around. Finally, paste the line AC-B in Fig.5(b) to the line GH, as shown in Fig.5(c). We call the resulting structure a *folded strip*. It is 2-dimensional. The crucial part of this structure is around the line DF-E. At this junction, two surfaces *tangential* to each other merge into one. Everywhere else the folded strip is locally homeomorphic to a 2-dimensional plane.

Our goal is to prove that trajectories on a folded strip can be chaotic. Suppose (a) there is a continuous vector field (with no equilibrium points) on the folded strip and the edges G-I-DF-AC and H-J-DF-AC of the strip are in parallel with this vector field; (b) the trajectory travels clockwise on this strip. Let us investigate the behavior of trajectories on this folded strip. Again, let us introduce a 1-dimensional map which is denoted by f_2 for this case. Using the same coordinate as before ($x_G = 0$ and $x_H = 1$), from Fig.5(c) we can see that the trajectory starting from the point G will go through points I and D and return to the point G. This means that we have $f_2(0) = 0$. Observe, however, that the trajectory starting from the point H will go through points J and F and return to the point G, also. This means that we have $f_2(1) = 0$. Clearly, there must be some critical point x^* between G and H (i.e. $0 < x^* < 1$), such that the trajectory starting from x^* will go through the point E (which is at the bottom of the strip) and arrive at the point B. Since point B is identified with the point H, we have $f_2(x^*) = 1$. From continuity we know f_2 is increasing for $x \in (0, x^*)$ and decreasing for $x \in (x^*, 1)$. Hence, f_2 is a unimodal map, as shown in Fig.6(c). There are many examples as well as rigorous proofs that a unimodal map can be chaotic([8][9]). Since the trajectories on a folded strip behave like a unimodal map, we have proved that they are potentially chaotic.

[Figure 5]

[Figure 6]

Now let us relate the folded strip structure to our attractor. From our observations, the folded junction structure actually exists in the attractor. Indeed, if we look at a sequence of consecutive Poincare cross-sections of the attractor, we can identify the folded junction structure. Here we give four consecutive Poincare cross-sections. Figure 7 shows the Poincare cross-sections at $v_2 = 0.9, 0.6, 0.3$ and 0, respectively. Each Poincare cross-section has two branches. Here we plot only the branch associated with the folded junction structure. In order to see the fine details, we have magnified the cross-sections. The readers can locate their corresponding positions in Fig.2 by comparing the coordinates.

[Figure 7]

The trajectory traverses in a clockwise direction on the $v_1 - v_2$ and $v_1 - i_3$ projections and in a counter-clockwise direction on the $v_2 - i_3$ projection. In Fig.7(a)(i.e. $v_2 = 0.9$), the cross-section has just started to fold. In Fig.7(b)(i.e. $v_2 = 0.6$), the cross-section has folded further to form an acute angle. In Fig.7(c)(i.e. $v_2 = 0.3$), the cross-section has almost completely folded. If we examine it carefully, we find that it is still "open" at the upper-right corner of the picture and therefore there is still a small angle. Finally, in Fig.7(d)(i.e. $v = 0$), which is the magnification of the upper-right part of Fig.3, it has completely folded. No matter how much we zoom it, within the finite word-length limitation of our computer (DECstation3100) we have found that it remains a line and not an angle.

We can also extract the unimodal map mentioned earlier from our calculation. To plot this one-dimensional map, we use the same data points for plotting the Poincare cross-sections. For example, for the $v_2 = 0.9$ Poincare cross-section (see Fig.7(a)), we plotted the $v_1 \rightarrow v_1$ map, as shown in Fig.8. For each point on the curve, the abscissa is the v_1 value of a point of the Poincare cross-section and the ordinate is the v_1 value of the next point where the trajectory crosses the Poincare cross-section again. Figure 8 shows clearly a unimodal map. Since our attractor has the structure of a folded-strip, our preceding analysis of the folded strip is applicable and hence the unimodal map in Fig.8 explains the mechanism of the non-fractal chaotic attractor quite well.

[Figure 8]

5. Experimental Observation

We have also observed the same attractor experimentally in the laboratory using an electronic analog circuit.

Observe that the parameters in (3) involve *negative* R and C, and that these negative elements are not connected to a common node. There are techniques for realizing negative capacitors and inductors using GIC (Generalized Immitance Converter) consisting of operational amplifier circuits([10]). To realize the floating negative elements, we can use the grounded-to-floating converters which are also made of op-amp circuits([11]). Although such a circuit can be designed and built, it becomes quite cumbersome that we opted for an *analog* circuit realization of Eq.(1).

Figure 9 shows the block diagram of our analog circuit. Observe that there are 4 types of building blocks in Fig.9; namely, linear amplifiers, integrators, summers and a nonlinear function generator. The circuits for implementing linear amplifier, integrator and summer are standard, as shown in Fig.10(a) (b) and (c), respectively. The only block which needs special design is the nonlinear function generator $f(\cdot)$. Figure 10(d) shows a realization of a nonlinear function generator, whose transfer characteristic is shown in Fig.10(e). With Fig.10(a), (c) and (d) as building blocks, the piecewise-linear characteristic in Fig.1(b) with any slopes G_a and G_b can be easily obtained.

The number of op-amps needed in this analog circuit realization is less than that required by the "physical circuit" approach. In addition, our analog circuit has other advantages. For example, since the variable i_3 is converted to a voltage signal in the analog circuit, it can be measured more easily without affecting the behavior of the system.

Figure 9

Figure 10

We have built a realization of Eq.(1) using the block diagram in Fig.9. Each block is realized using the basic structures in Fig.10, or their combinations. After choosing an appropriate normalizing scale, we found that for the parameter values close to those in Eq.(3), the same attractor is observed as that obtained from computer simulation. Figure 11 gives the oscilloscope pictures of $v_1 - v_2$, $v_1 - i_3$ and $v_2 - i_3$ projections of the attractor, respectively. They are qualitatively identical to the results

obtained from computer simulation (see Fig.2). Figure 12 shows the spectrum of $v_1(t)$ obtained from an HP3582A spectrum analyzer. Again, it is similar to the numerical result shown in Fig.4.

$$\boxed{\text{Figure 11}}$$

$$\boxed{\text{Figure 12}}$$

6. Discussion on Dimension

The fractal dimension is often used as another characterizing feature of a chaotic attractor. There are many definitions for various types of dimension. Some of them are only of theoretical interest because they are impractical from a computational point of view.

In practice, the so-called *Lyapunov dimension* is widely used because it is related to the Lyapunov exponents by a simple formula. Once the Lyapunov exponents of an attractor are calculated, the Lyapunov dimension is a by-product of the calculation. Its definition is as follows. Let $l_1 \geq \cdots \geq l_n$ be the Lyapunov exponents of an attractor of a continuous-time dynamical system. Let j be the largest integer such that $l_1 + \cdots + l_j \geq 0$. The Lyapunov dimension d_l is defined as

$$d_l = j + \frac{l_1 + \cdots + l_j}{|l_{j+1}|} \tag{6}$$

In the case of a 3-dimensional vector field where the three Lyapunov exponents l_1, l_2 and l_3 satisfy

$$l_1 \geq l_2 \geq 0 > l_3 \tag{7}$$

the formula for calculating the Lyapunov dimension d_l is given simply by

$$d_l = 2 + \frac{l_1 + l_2}{|l_3|} \tag{8}$$

Yorke and others have classified different definitions of dimensions into two broad categories; namely, *metric dimensions* and *frequency-dependent dimensions*. All metric dimensions tend to yield the same value, which is called the *fractal dimension* and denoted by d_F. Similarly, all probabilistic dimensions tend to yield the same value, which is called the dimension of the *natural measure* and denoted by d_μ. Typically, $d_\mu < d_F$. Formula (6) was originally given by Yorke and Kaplan and they

conjectured that the Lyapunov dimension d_l is equal to the dimension of the natural measure d_μ and is a *lower* bound on the fractal dimension d_F ([4][12]).

The Lyapunov exponents of our attractor, as listed in (4), satisfy condition (7). According to (8), its Lyapunov dimension is

$$d_l = 2 + \frac{0.0345}{0.755} = 2.0457$$

The capacity dimension, which is one of the metric dimensions, can be calculated by

$$d_{cap} = \lim_{\varepsilon \to 0} \frac{\ln N(\varepsilon)}{\ln(1/\varepsilon)} \qquad (9)$$

where ε is the diameter of a small volume element(sphere, cube, etc.) and $N(\varepsilon)$ is the minimum number of such volume elements needed to cover an attractor. Since our attractor is located on a 2-dimensional surface, its capacity dimension d_{cap} is at most 2. From Fig.3 and Fig.7 we can see the attractor's cross-sections are continuous curves, which indicate that $d_{cap} = 2$ for this attractor.

We can also calculate the correlation dimension for this attractor. The correlation dimension d_{cor} is defined by

$$d_{cor} = \lim_{\varepsilon \to 0} \frac{\ln \sum_{i=1}^{N(\varepsilon)} P_i^2}{\ln \varepsilon} \qquad (10)$$

where ε and $N(\varepsilon)$ have the same meaning as in Eq.(9) and P_i is the relative frequency with which a typical trajectory enters the ith volume element. From its definition we know that d_{cor} belongs to the category of a frequency-dependent dimension. To numerically calculate d_{cor}, one can use the *correlation integral* $C(\varepsilon)$ defined by

$$C(\varepsilon) = \lim_{N \to \infty} \frac{1}{N^2} \{ \text{ the number of pairs of points } (x_i, x_j) \qquad (11)$$

$$\textit{such that } ||x_i - x_j|| < \varepsilon\}$$

where N is the total number of points of a trajectory. It can be shown that ([6])

$$C(\varepsilon) = \sum_{i=1}^{N(\varepsilon)} P_i^2$$

Therefore the algorithm for calculating the correlation dimension is efficient and relatively easy to implement on a computer. In INSITE there is a subprogram for calculating the correlation dimension. Using data number $N = 50000$, the result of our

calculation is shown in Fig.13. The horizontal axis is $\log_2(\varepsilon/\varepsilon_0)$, where ε_0 is a small constant in the program. The vertical axis is $\log_2 C(\varepsilon)$. In practice, the $\log_2 C(\varepsilon)$ - $\log_2(\varepsilon/\varepsilon_0)$ curve is nearly a straight line in a portion of the curve and the slope of this line is the correlation dimension([6]). For the line shown in Fig.13, we have $d_{cor} = 1.98$.

<div align="center">

[Figure 13]

</div>

The two dimensions d_{cap} and d_{cor} are related by

$$d_{cor} \leq d_{cap}$$

where the equality holds only when the trajectory visits each point on its attractor at a uniform probability (i.e. the trajectory is ergodic). Indeed, when we have

$$P_i = \frac{1}{N(\varepsilon)} \qquad \text{for all } i = 1, 2, \cdots , N(\varepsilon) ,$$

Eq.(10) becomes

$$d_{cor} = \lim_{\varepsilon \to 0} \frac{\ln \sum_{i=1}^{N(\varepsilon)} \frac{1}{[N(\varepsilon)]^2}}{\ln \varepsilon} = \lim_{\varepsilon \to 0} \frac{-\ln N(\varepsilon)}{\ln \varepsilon} = d_{cap}$$

Hence $d_{cor} = 1.98 \approx 2$ is a very interesting numerical result. It means that our attractor is nearly ergodic on the 2-dimensional surface, as can be seen from Fig.2.

Therefore, both theoretical analysis and numerical calculation have shown that our present attractor has $d_{cor} \leq d_{cap} \leq 2$. However, since it has a positive Lyapunov exponent, its Lyapunov dimension $d_l > 2$. So our attractor seems to provide a counter-example to the Kaplan-Yorke conjecture.

7 Conclusions

(1) A 2-dimensional surface with a special geometrical structure called a folded strip is introduced. Using a 1-dimensional map, it is proved that trajectories on a folded strip can be chaotic.

(2) In a 3-rd order autonomous piecewise-linear circuit, we have observed both numerically and experimentally a chaotic attractor which has the structure of the folded strip.

(3) The attractor is chaotic but non-fractal. Its capacity dimension d_{cap} is equal to 2 and the correlation dimension d_{cor} is less than but very nearly equals to 2. On

the other hand, since it has a positive Lyapunov exponent, its Lyapunov dimension is greater than 2. Hence, the Kaplan-Yorke conjecture does not hold for this attractor.

(4) The folded strip may be only one of many possible *2-dimensional surfaces* on which a trajectory in a 3-dimensional space can be chaotic. Hence, other non-fractal chaotic attractors may also exist in 3-dimensional vector fields.

References

[1] C. Grebogi, E. Ott, S. Pelikan and J. A. Yorke, "Strange attractors that are not chaotic", *Physica* 13D pp.261-268, 1984.

[2] C. Grebogi, E. Ott and J. A. Yorke, "Attractors on an N-torus: quasi-periodicity versus chaos", *Physica* 15D pp.354-373, 1985.

[3] L. O. Chua and G. N. Lin, "Canonical realization of Chua's circuit family," *IEEE Trans. on Circuits and Systems,* vol. CAS-37, pp. 885-902, July. 1990.

[4] J. D. Farmer, E. Ott and J. A. Yorke, "The dimension of chaotic attractors", *Physica* 7D pp.153-180, 1983.

[5] T. S. Parker and L. O. Chua, "INSITE-A software toolkit for the analysis of non-linear dynamical systems", *Proceedings of the IEEE,* vol. 75, no.8, pp.1081-1089, Aug. 1987.

[6] T. S. Parker and L. O. Chua, *Practical numerical algorithms for chaotic systems,* Spring-Verlag 1989.

[7] H. Haken, "At least one Lyapunov exponent vanishes if the trajectory of an attractor does not contain a fixed point", *Physics Letters* A 94, pp.71-72, 1983.

[8] P. J. Holmes and D. C. Whitley, "Bifurcations of one- and two- dimensional maps", *Phil. Trans. Roy. Soc. Lond.,* vol A311, pp 43-102, 1984.

[9] P. Collet and J. P. Eckmann, *Iterated maps on the interval as dynamical systems,* Birkhauser, 1980.

[10] L. T. Bruton, *RC-Active Circuits: Theory and Design,* Englewood Cliffs, 1980.

[11] L. O. Chua and S. Wong, "Synthesis of piecewise linear networks", *IEEJ Electronic Circuits and Systems,* vol.2, pp.102-108, 1978.

[12] J. Kaplan and J. Yorke, "Functional equations and the approximation of fixed points", Proceedings, Bonn, July, 1978, *Lecture Notes in Math.* H.O. Peitgen and H.O. Walther, eds., (Springer, Berlin, 1978), p.228.

Figure captions

Fig.1 (a) The canonical realization of the Chua's circuit family.

(b) The v-i characteristic of the nonlinear resistor G_N.

Fig.2 Trajectories of the system (1) with the parameter values given by (3).

(a) Projection on $v_1 - v_2$ plane. The trajectory travels in a clockwise direction.

(b) Projection on $v_1 - i_3$ plane. The trajectory travels in a clockwise direction.

(c) Projection on $v_2 - i_3$ plane. The trajectory travels in a counter-clockwise direction.

Fig.3 The Poincare cross-section at the $v_2 = 0$ plane.

Fig.4 The spectrum of the waveform $v_1(t)$ of the attractor in Fig.2.

Fig.5 (a) A flat strip; (b) A folded junction; (c) A folded strip.

Fig.6 (a) A monotone-increasing map;

(b) A monotone-decreasing map;

(c) A unimodal map.

Fig.7 A sequence of successive Poincare cross-sections showing the folded junction structure of the attractor.

(a) At $v_2 = 0.9$ plane;

(b) At $v_2 = 0.6$ plane;

(c) At $v_2 = 0.3$ plane;

(d) At $v_2 = 0$ plane;

Fig.8 A unimodal map obtained from the data of the $v_2 = 0.9$ Poincare cross-section.

Fig.9 The block diagram of the system described by Eq.(1).

Fig.10 (a) Realization of a linear amplifier;

(b) Realization of an integrator;

(c) Realization of a summer;

(d) Realization of the nonlinear function generator $f(\cdot)$.

Fig.11 The oscilloscope pictures of the attractor.

(a)$v_1 - v_2$ projection; (b)$v_1 - v_3$ projection; (c)$v_2 - v_3$ projection.

Fig.12 The measured spectrum of the waveform of v_1.

Fig.13 The correlation dimension of the attractor.
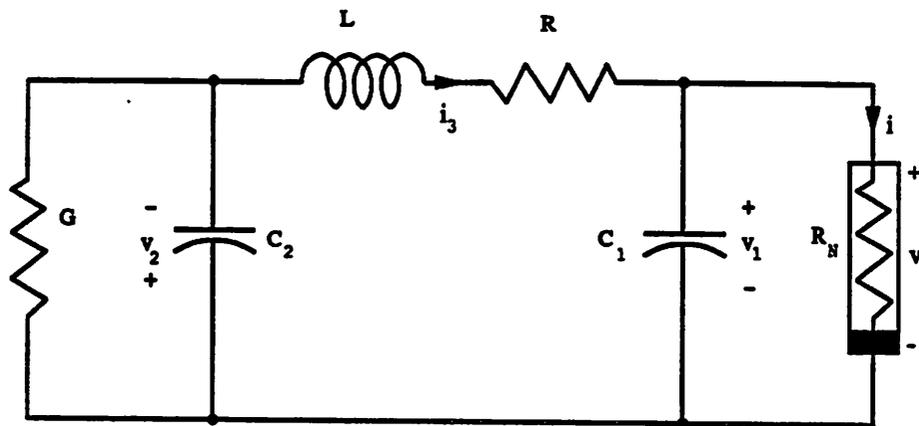
Fig.1(a)
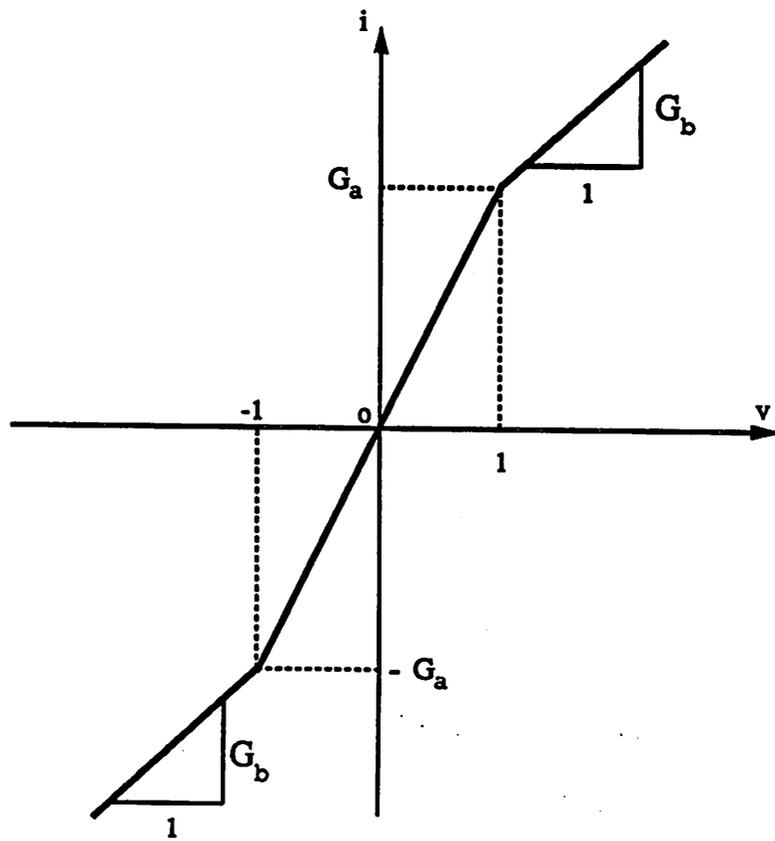
Fig. 1(b)
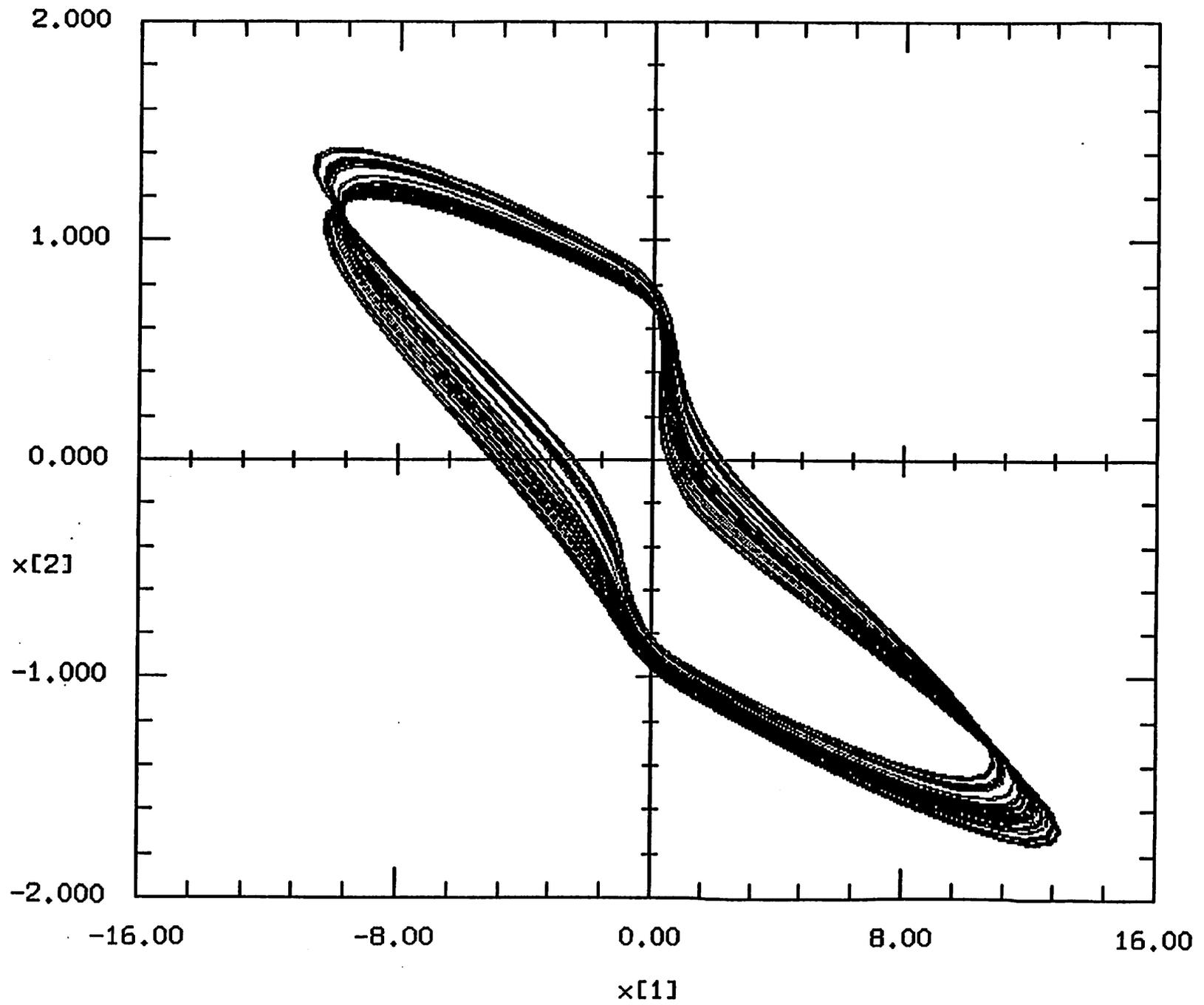
Fig.2(a)
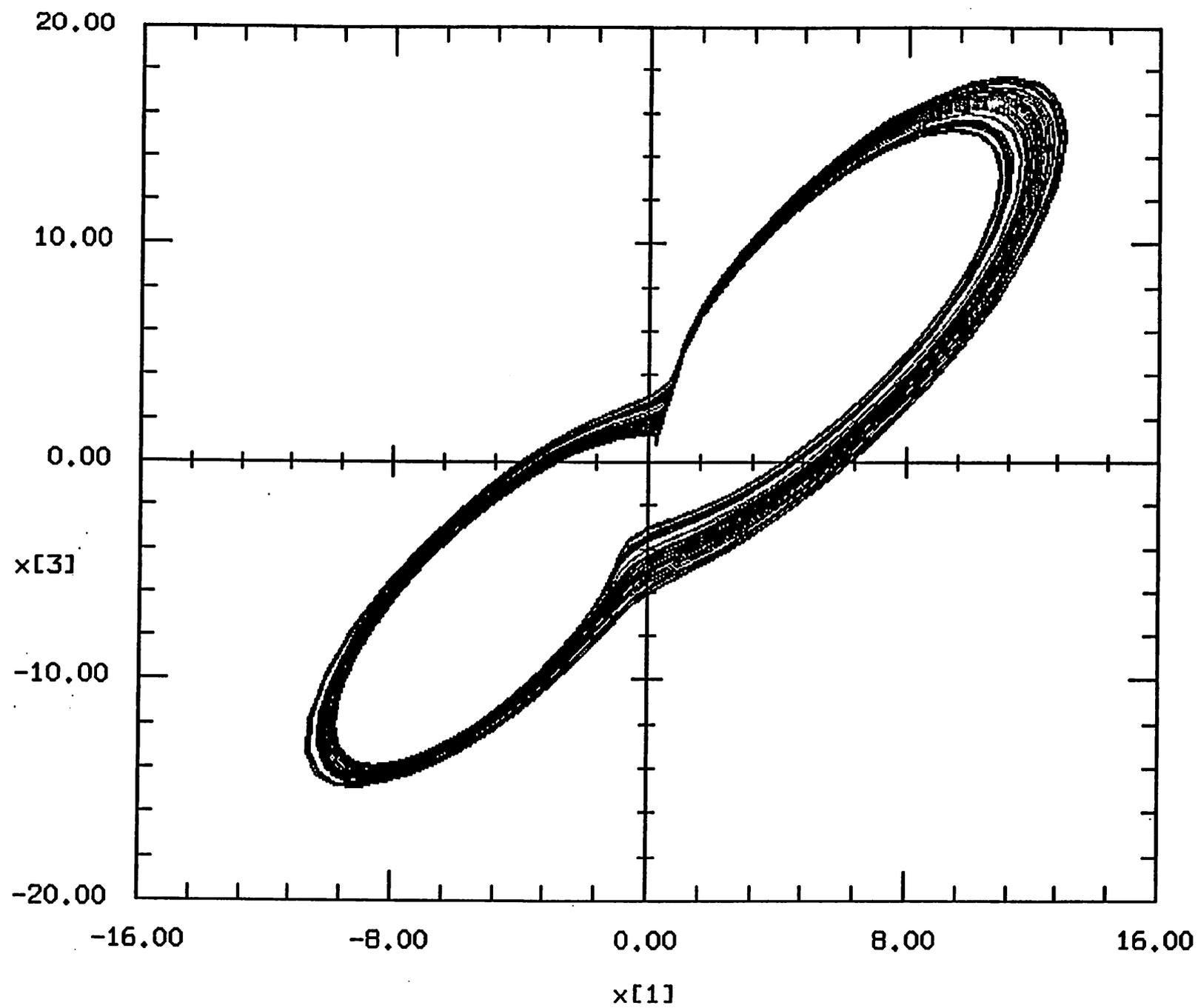
Fig.2(b)
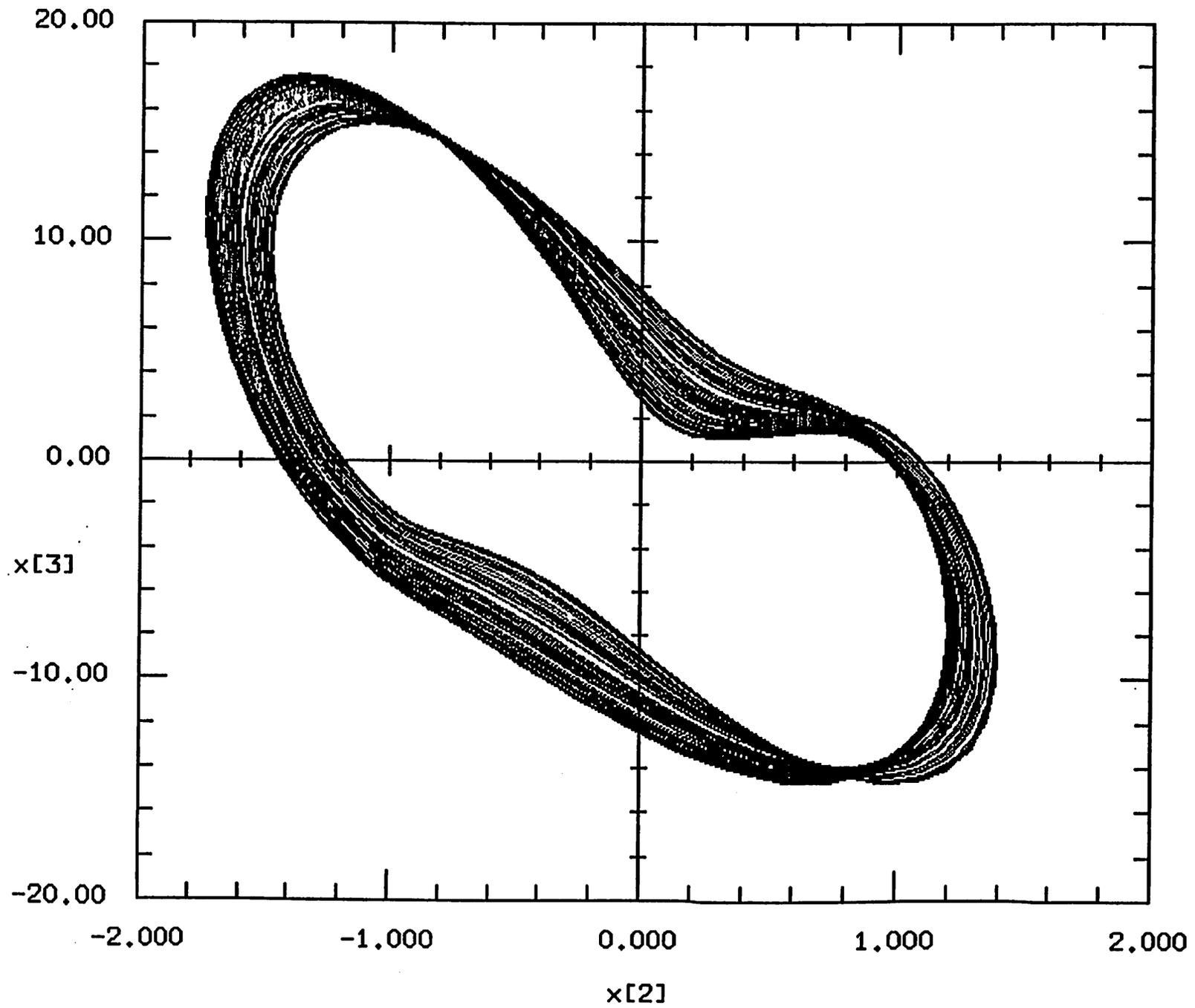
Fig.2(c)

Fig.3

magnitude (dB)

Fig.4

(a)

C   F   J   H x

1

x_1

x_1

B   E x_0

x_1'

A   D   I   G   0

(b)

AC   DF   J   H

B   E   I   G

(c)

BH x^* ACG

J   I

DF

E

Fig.5

(a)

(b)

(c)
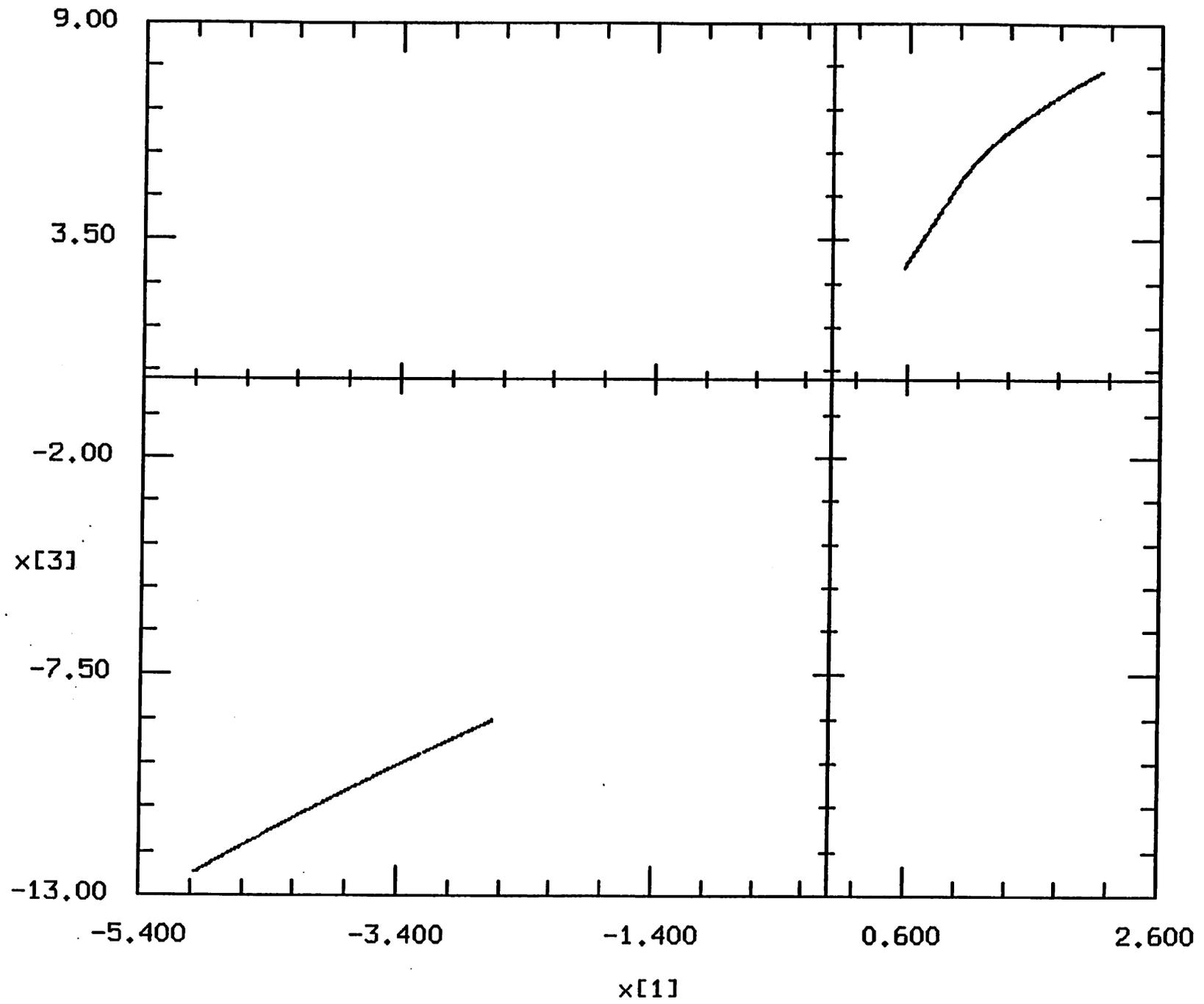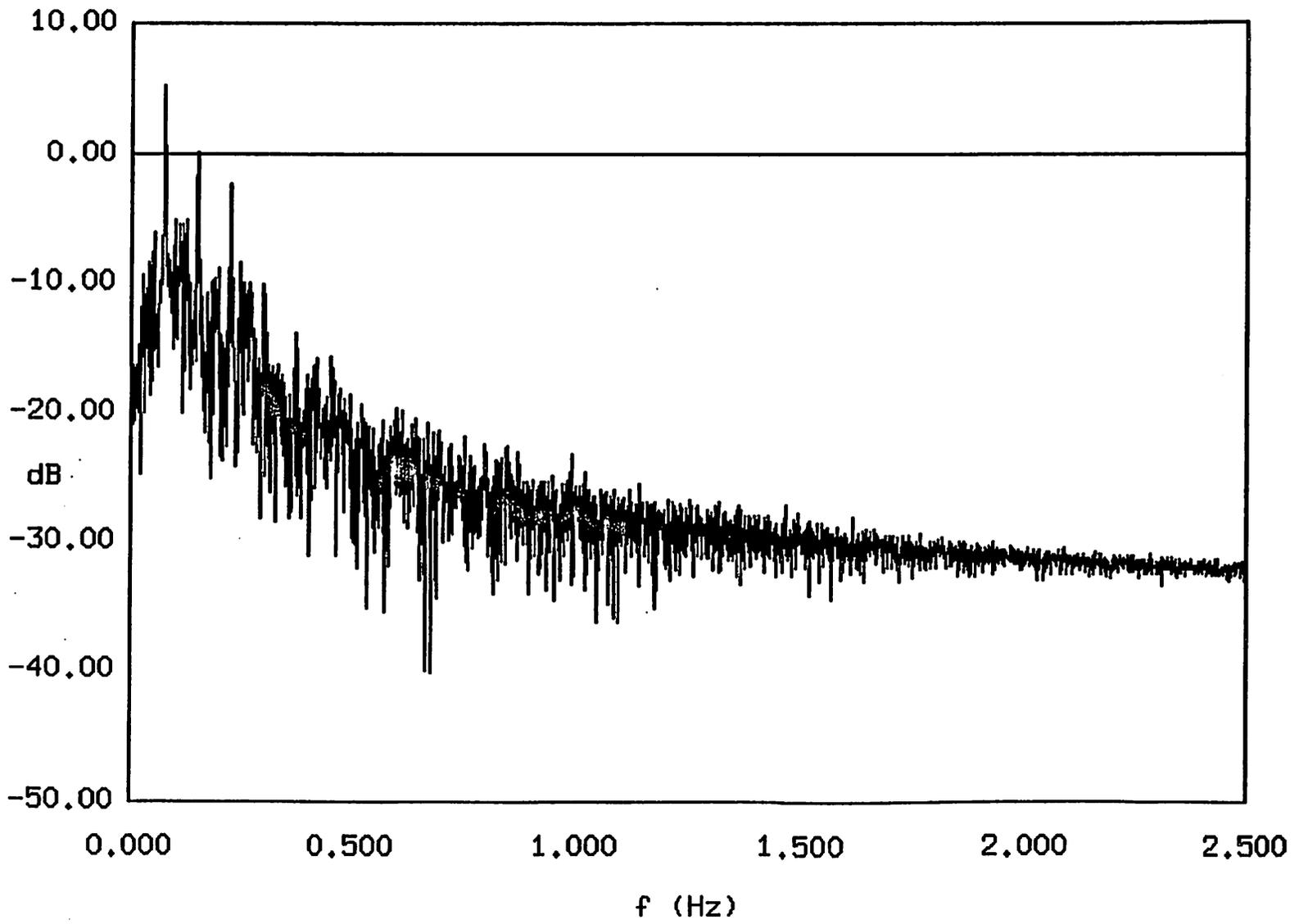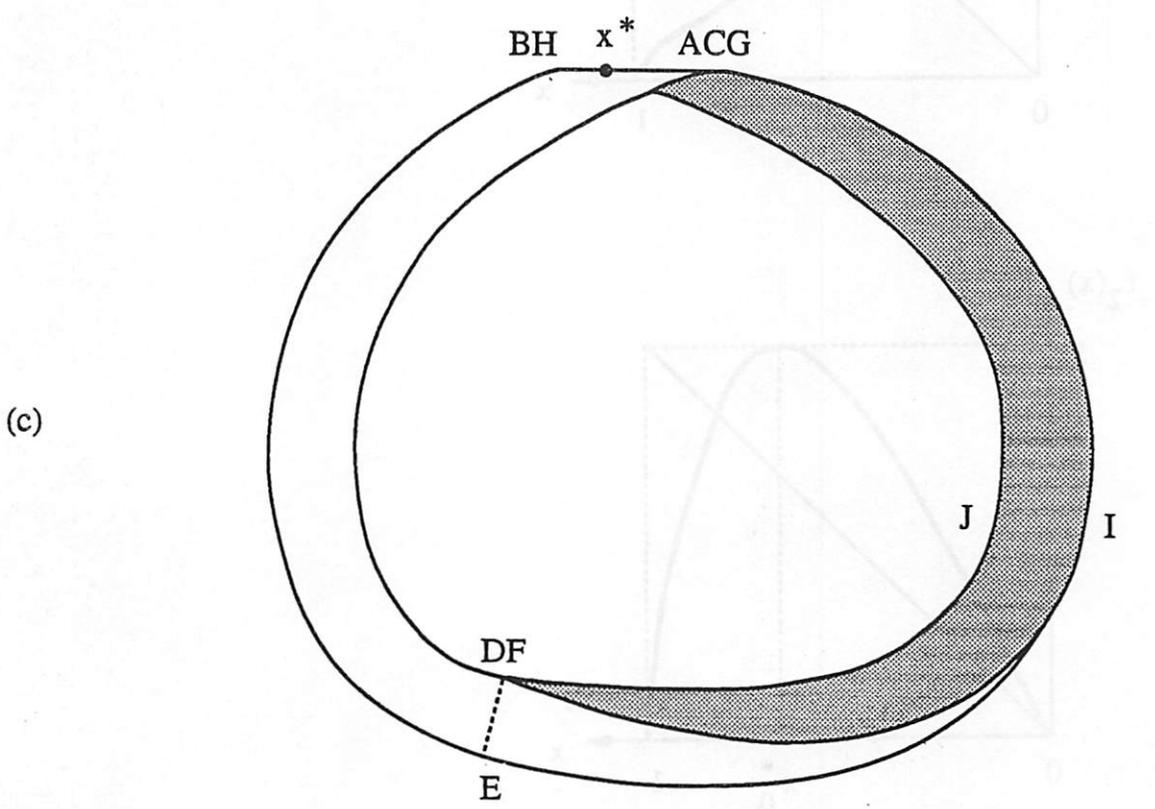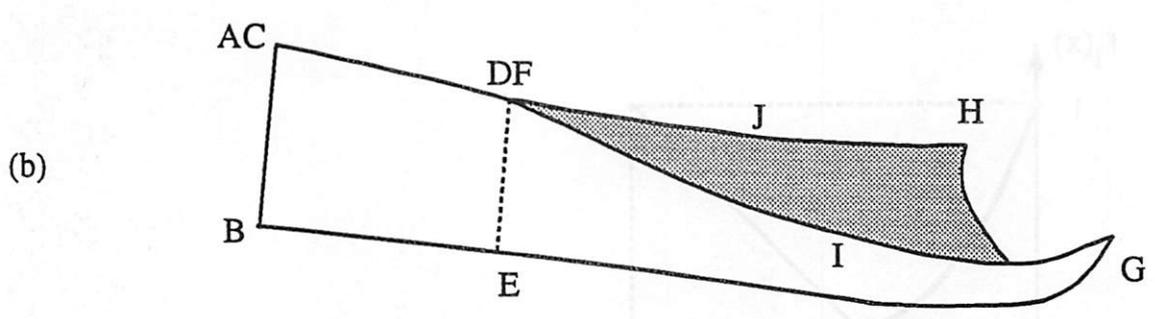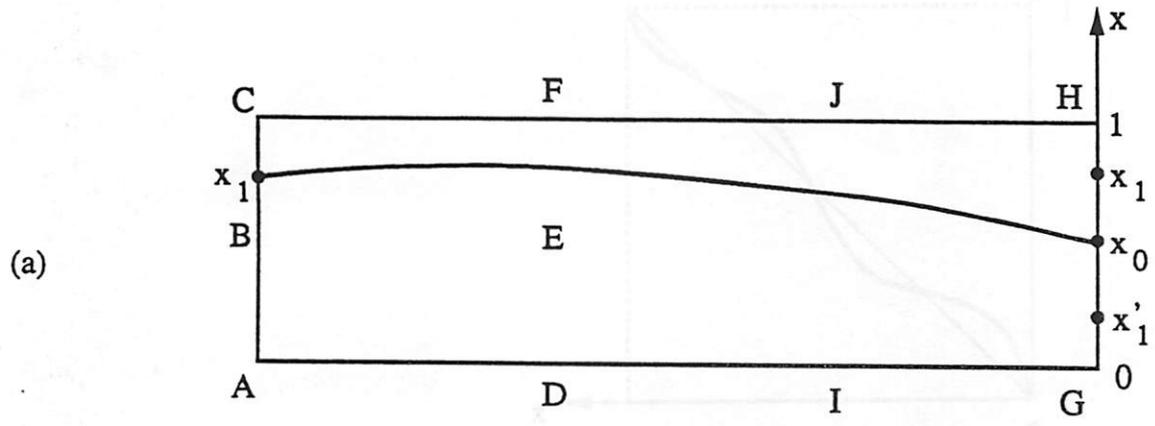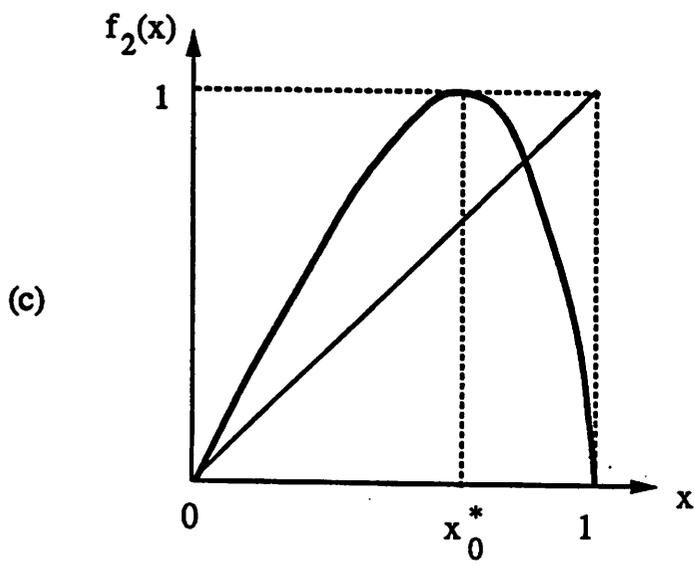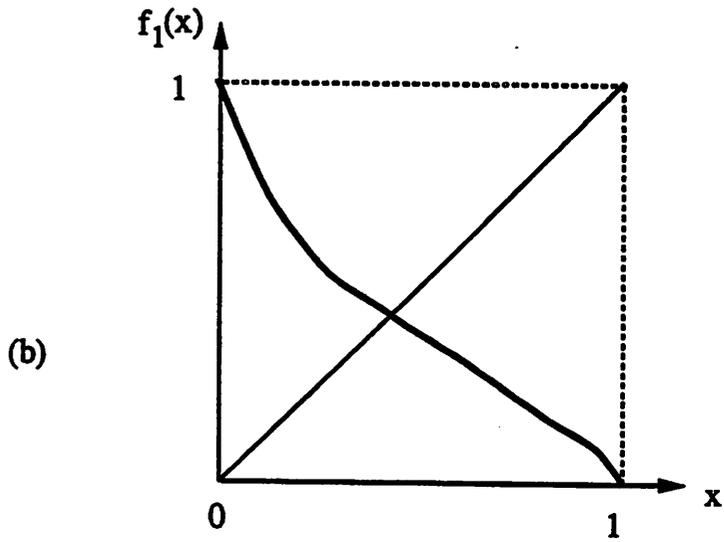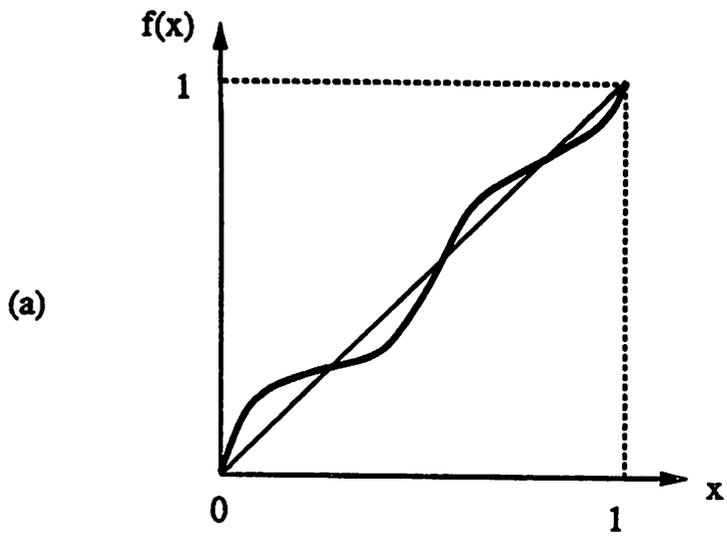
Fig.6
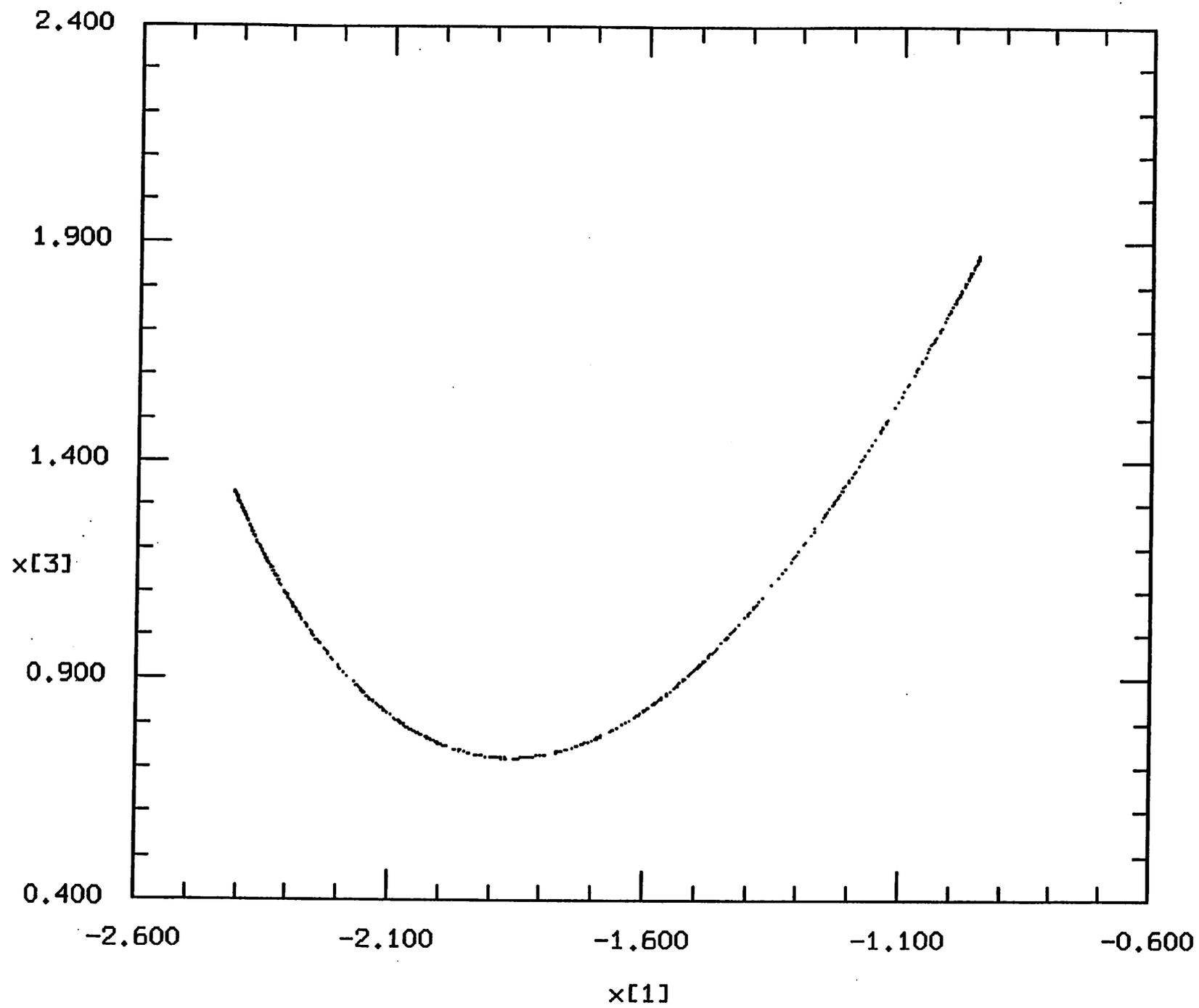
Fig.7(a)
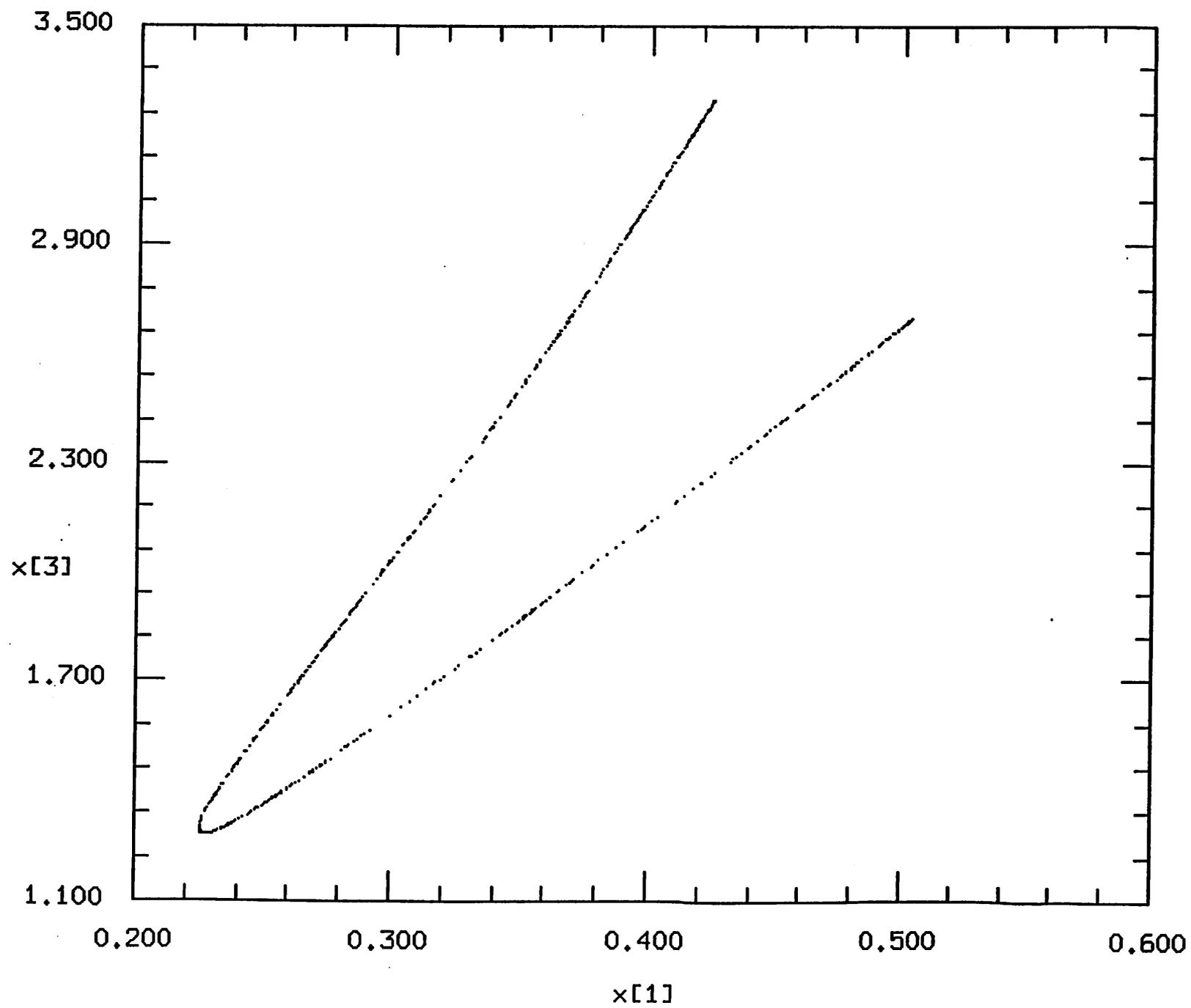
Fig.7(b)
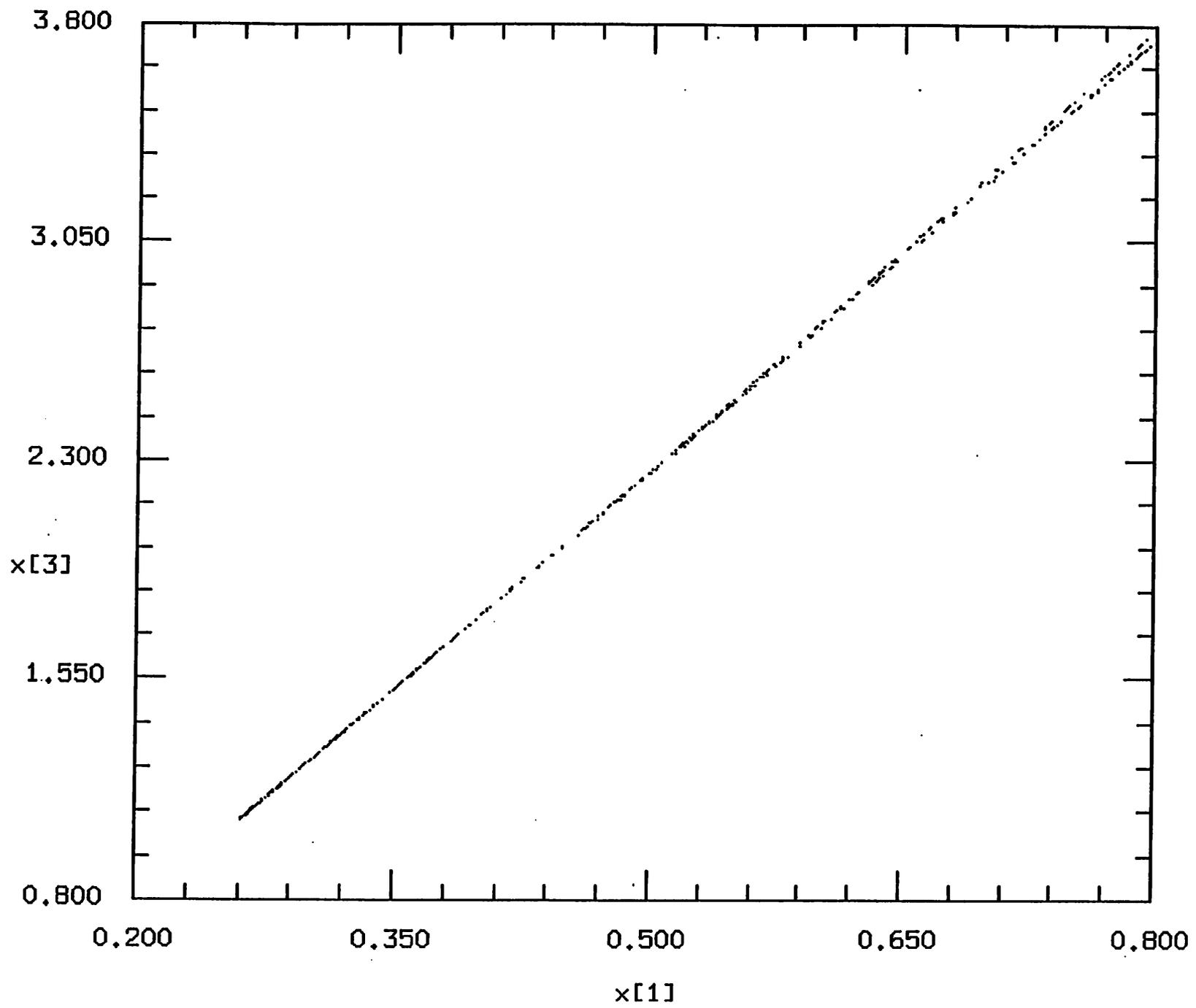
Fig.7(c)
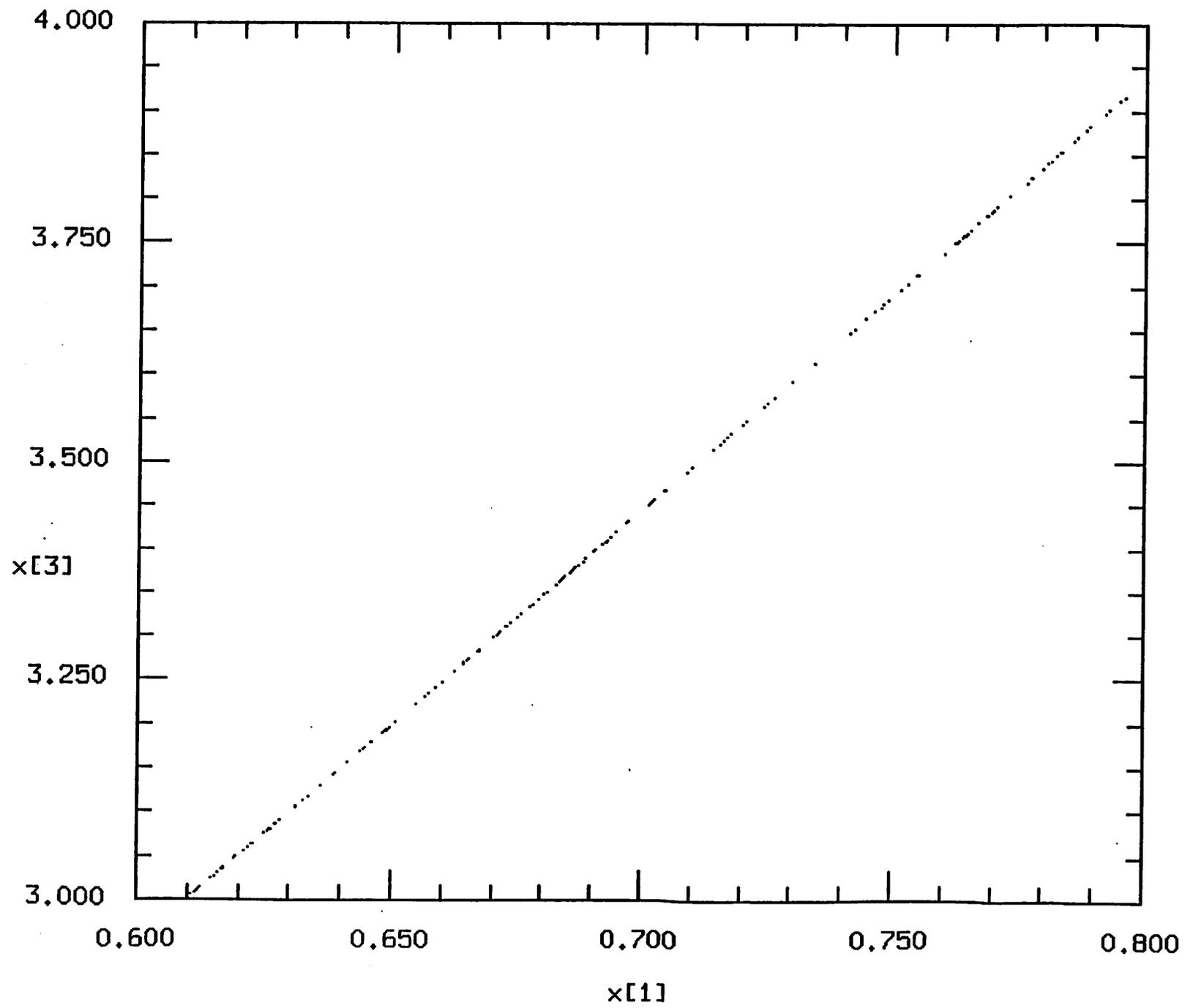
Fig.7(d)
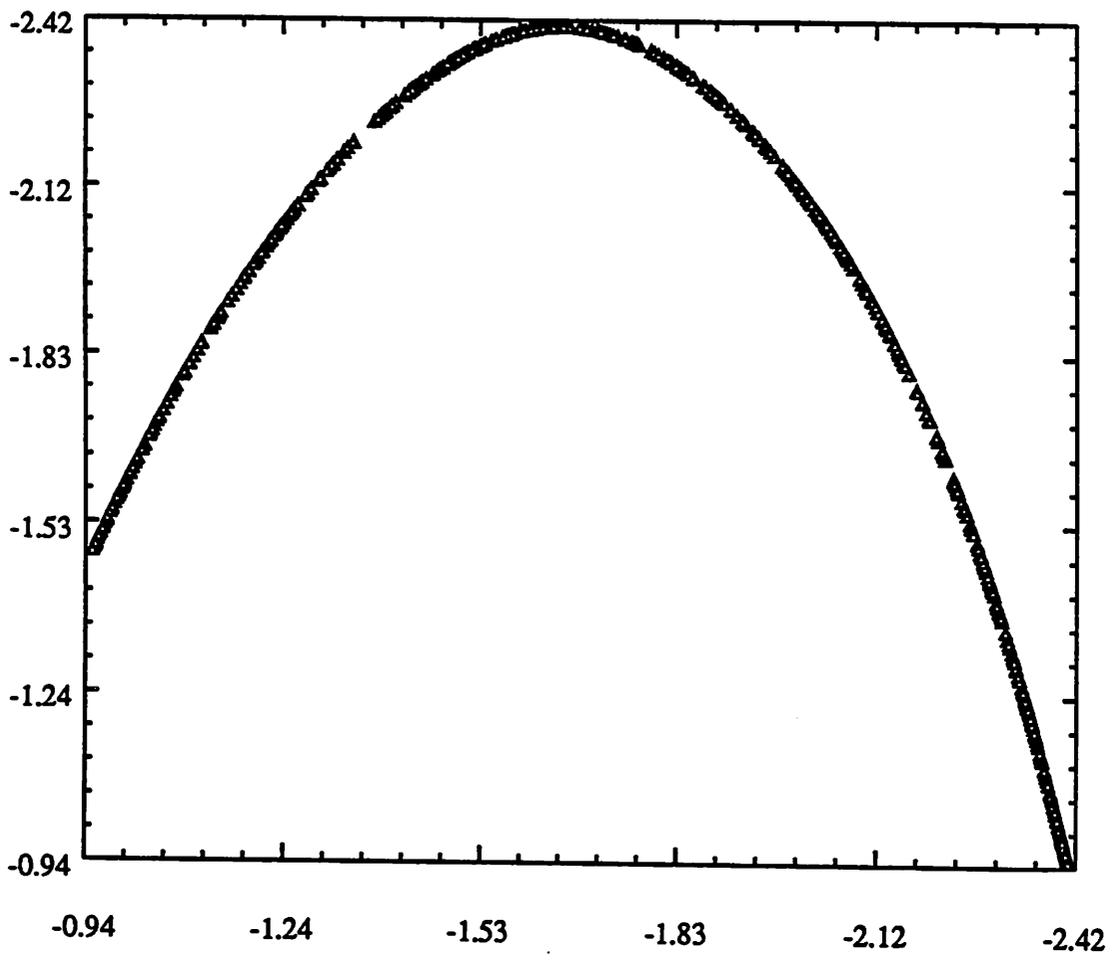
Fig.8
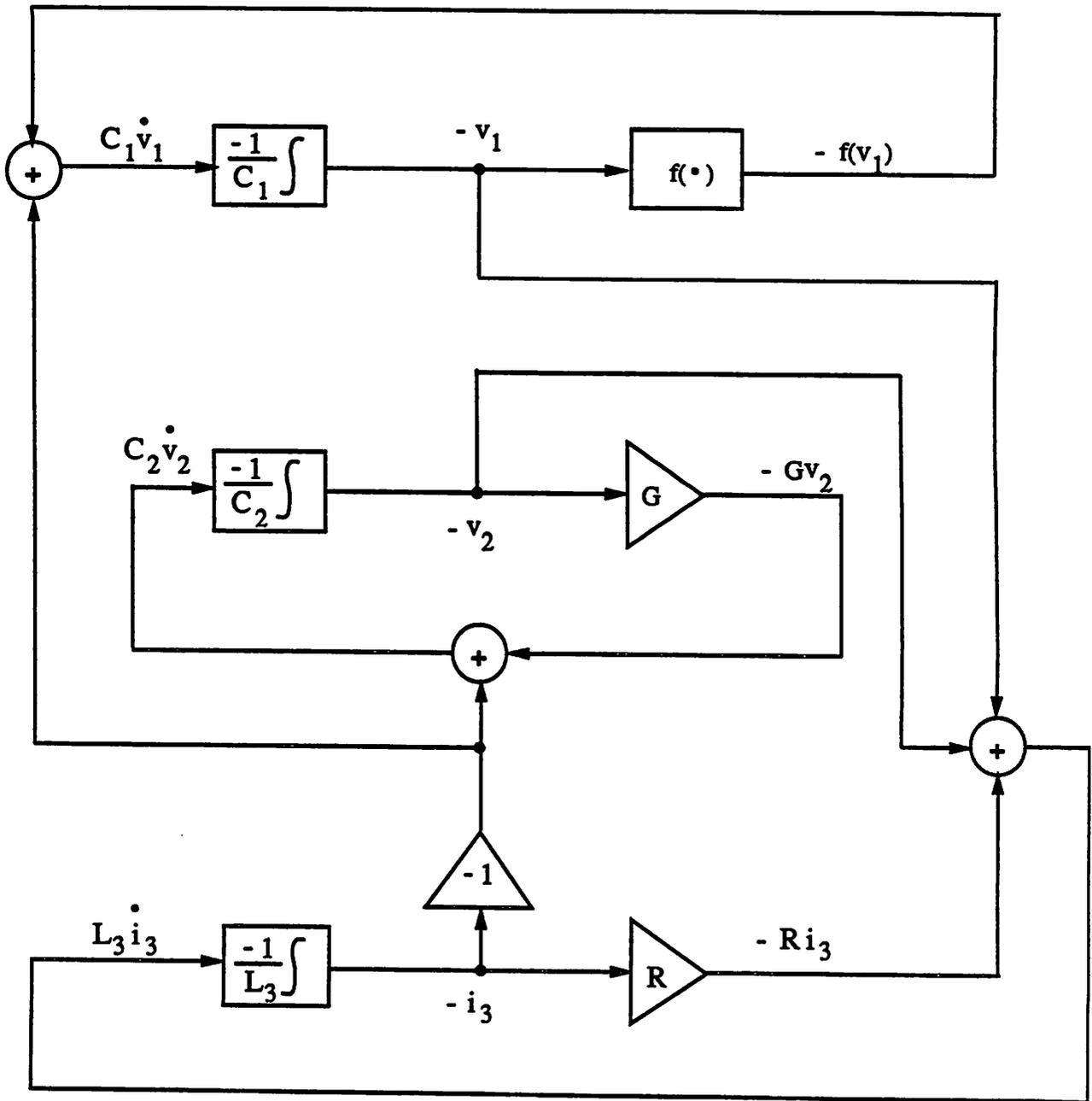
Fig.9
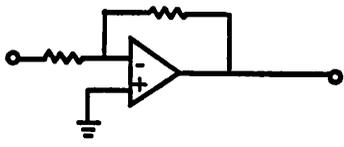
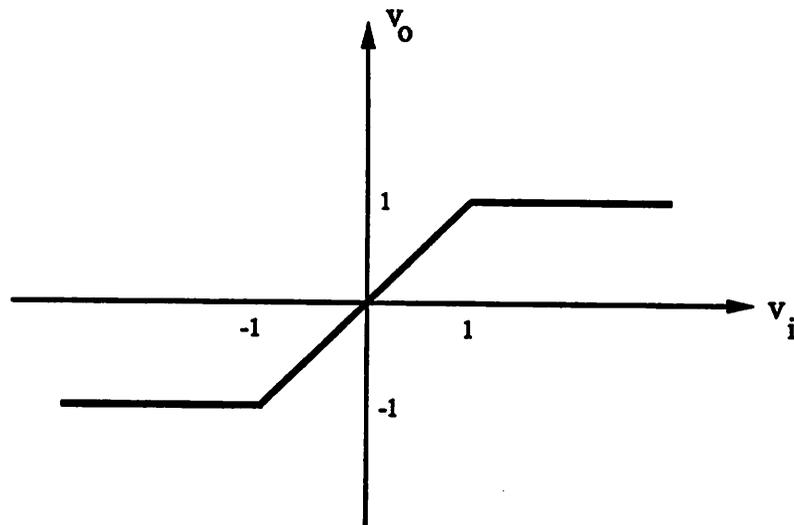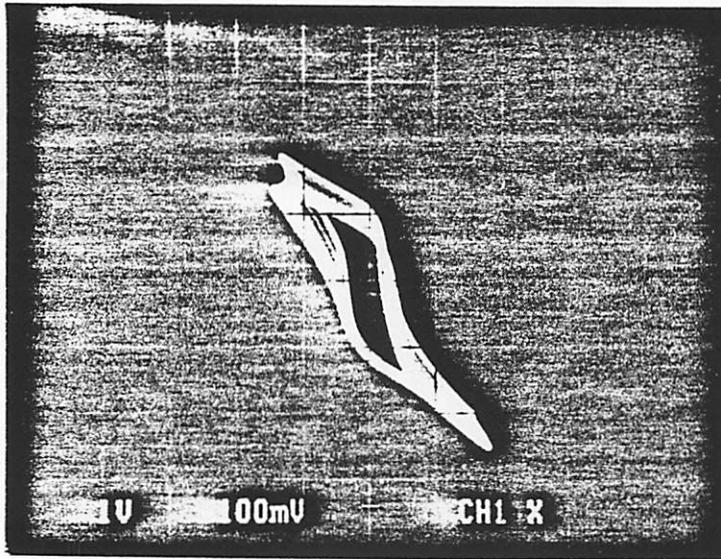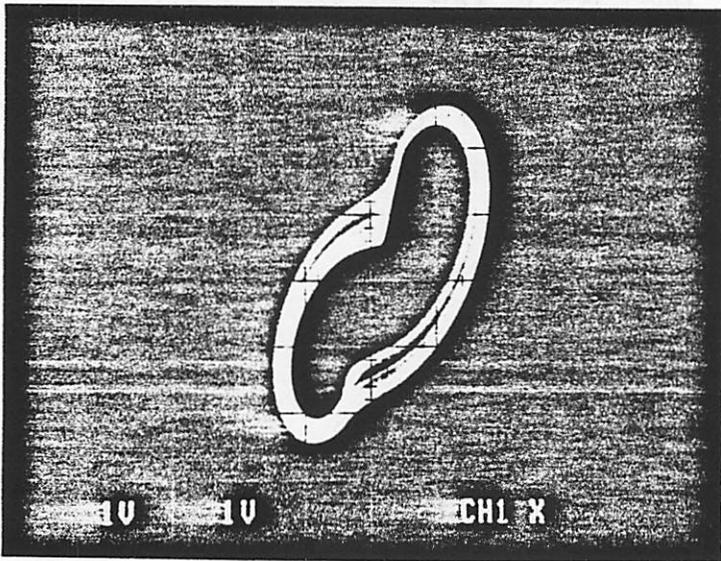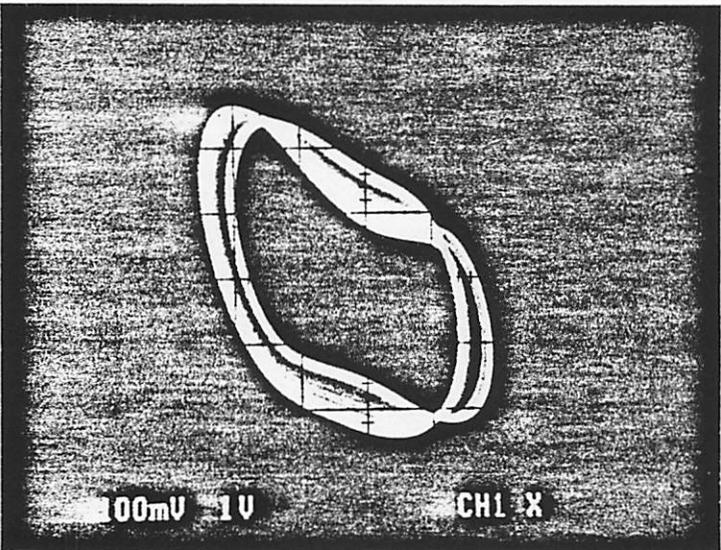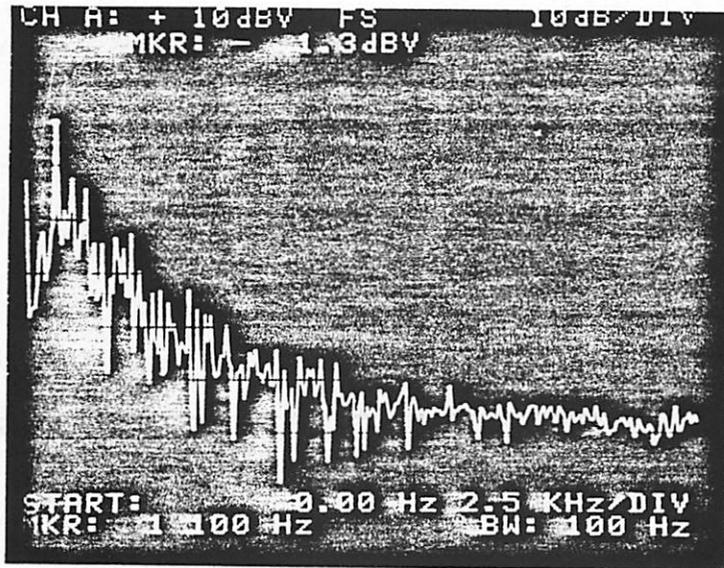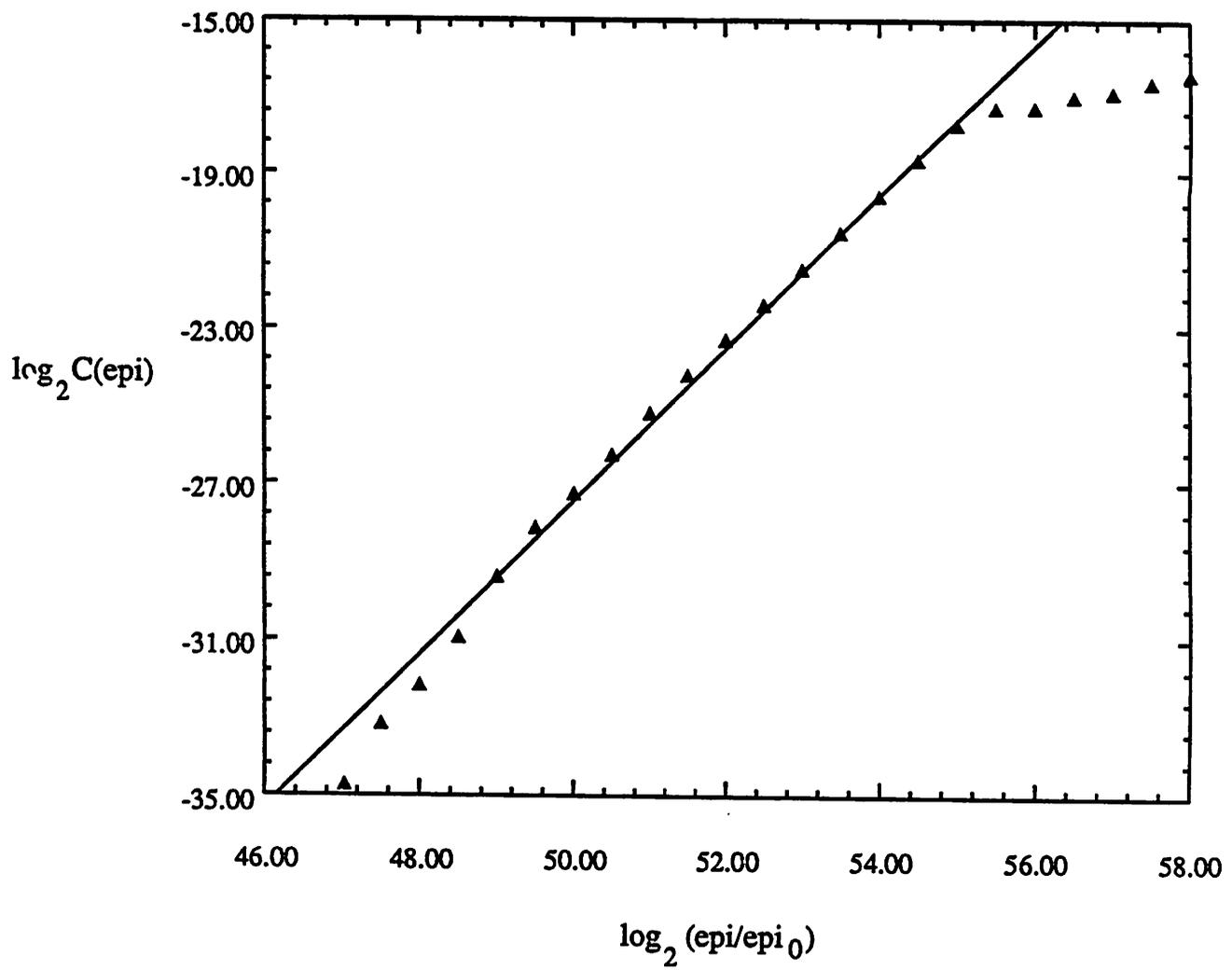(a)
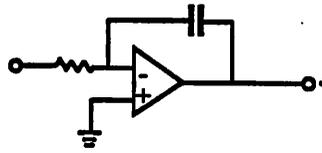
(b)
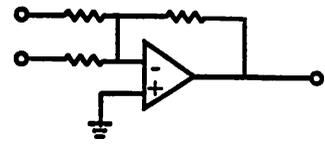
(c)
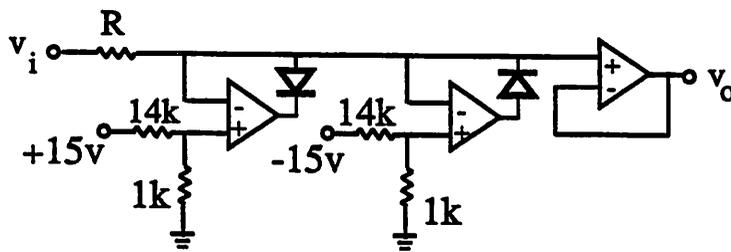
(d)

(e)

Fig.10

(a)

(b)

(c)

Fig.11

Fig.12

Fig 12

Fig.13